Structural Hierarchy in Flow-Aligned Hexagonally Self-Organized Microphases with Parallel Polyelectrolytic Structures

Teemu Ruotsalainen,[†] Mika Torkkeli,[‡] Ritva Serimaa,[‡] Tapio Mäkelä,[§] Riikka Mäki-Ontto,[†] Janne Ruokolainen,[†] Gerrit ten Brinke,*[,⊥] and Olli Ikkala*[,†]

Department of Engineering Physics and Mathematics and Center for New Materials, Helsinki University of Technology, P.O. Box 2200, FIN-02015, Finland; Department of Physical Sciences, University of Helsinki, P.O. Box 64, FIN-00014, Finland; VTT Information Technology, Microelectronics, P.O. Box 1208, FIN-02044 VTT, Finland; and Department of Polymer Science and Materials Science Center, University of Groningen, Nijenborgh 4, 9747 AG Groningen, The Netherlands

Received May 9, 2003; Revised Manuscript Received September 16, 2003

ABSTRACT: We report a novel structural hierarchy where a flow-aligned hexagonal self-organized structure is combined with a polyelectrolytic self-organization on a smaller length scale and where the two structures are mutually parallel. Polystyrene-*block*-poly(4-vinylpyridine) (PS-*block*-P4VP) is selected with a short P4VP block, which is protonated with *p*-toluenesulfonic acid (TSA) and further hydrogen bonded with 3-*n*-pentadecylphenol (PDP). To suppress the amount of free (uncomplexed) acid which we expected to have adverse effects during the extended shearing at the elevated temperatures, a safely less than stoichiometric amount of TSA was used, i.e., PS-*block*-P4VP(TSA)$_{0.9}$(PDP)$_{1.0}$. The formation of the supramolecules and the resulting structures were investigated using infrared spectroscopy (FTIR), small-angle X-ray scattering (SAXS), and transmission electron microscopy (TEM). As the weight fraction of P4VP(TSA)$_{0.9}$(PDP)$_{1.0}$ is ca. 20%, hexagonal self-organization occurs, as shown by SAXS. Shear flow leads to remarkably well-aligned structures. SAXS also indicates an internal structure within the P4VP(TSA)$_{0.9}$(PDP)$_{1.0}$ blocks with a long period of 41 Å. In contrast to the previously observed structural hierarchies in diblock copolymer/amphiphile supramolecules, which contained mutually perpendicular structures, e.g., lamellae within cylinders, in the present case SAXS in combination with models suggests internal polyelectrolytic layers parallel to the hexagonally ordered microphases. These aligned conducting nanochannels also manifest as a slight overall conductivity anisotropy.

1. Introduction

Self-organizing[1] polymers have been pursued to tailor the materials properties, functionalities, and even responsivity; see e.g. refs 2−5. Structural hierarchy can be useful in this respect, and different schemes have been reported based for example on (i) use of block copolymers with several blocks, such as ABC triblock copolymers and their blends,[6−10] (ii) incorporation of rodlike moieties within block copolymers,[2,11−16] (iii) use of polymeric supramolecules where repulsive moieties are bonded to block copolymers using physical interactions such as hydrogen bonding, charge transfer, or coordination,[17−22] or (iv) hydrogen bonding liquid crystals to block copolymers.[23] As an example closely related to the present work, if a diblock copolymer polystyrene-*block*-poly(4-vinylpyridine), PS-*block*-P4VP, is used and alkylphenol, such as pentadecylphenol (PDP) or nonadecylphenol (NPD), is hydrogen bonded selectively to P4VP, self-organizing comb-shaped supramolecular blocks P4VP(PDP) or P4VP(NPD) are formed.[17,18] The architecture formally corresponds to a triblock copolymer A-*block*-(B-*graft*-C) which opens a route to structural hierarchy, showing for example alternating P4VP and alkyl layers within cylinders in the glassy PS matrix, i.e., lamellae-*within*-cylinder structure.[18] Importantly, the lamellae have so far always been perpendicular to the direction of the cylinders even after shear orientation.[24] Also, the relative weight fractions of the blocks can be reversed, which leads to glassy PS cylinders within the P4VP(NDP)[18] or the P4VP(PDP)[25] matrix, and because of the plasticization of the latter phase, shearing leads to highly aligned PS cylinders and alignment in two length scales.[25] The structures have also in this case been mutually perpendicular.

Overall alignment of the local structures can be achieved in thin films by adjusting surface energies[26] and in thicker materials for example by external fields[27−31] or flow fields.[25,32−37] This will lead to materials with macroscopically anisotropic properties.

In this work we aim to study flow-aligned self-organized protonically conducting polyelectrolytic materials containing structural hierarchies. We have previously studied conductivity behavior in different compositions[37] and showed even switching.[17] In this work we use PS-*block*-P4VP with a very short P4VP block and use *p*-toluenesulfonic acid (TSA) to prepare the polyelectrolyte block P4VP(TSA) due to protonation (see Figure 1). TSA was selected as it is among the simplest aromatic sulfonic acids, and its aromatic structure leads to thermally stable complexes, as was found in the context of protonation of polyaniline.[38] PDP is complexed with P4VP(TSA), the aim being to obtain hydrogen bonding between the phenolic hydroxyls and the sulfonates. The structures are characterized using FTIR, SAXS, TEM, and ac conductivity measurements. Two observations will be underlined: First, shear orientation conditions were identified that allow hexagonal self-organization of the polyelectrolytic microphases with high overall alignment. Second, a novel

[†] Helsinki University of Technology.
[‡] University of Helsinki.
[§] VTT Information Technology, Microelectronics.
[⊥] University of Groningen.
* Corresponding authors: Tel +31-50-3634509; Fax +31-50-3634400; e-mail G.ten.Brinke@chem.rug.nl; Tel + 358-50-4100454; Fax +358-9-4513155; e-mail Olli.Ikkala@hut.fi.

10.1021/ma0345955 CCC: $25.00
Published on Web 11/14/2003

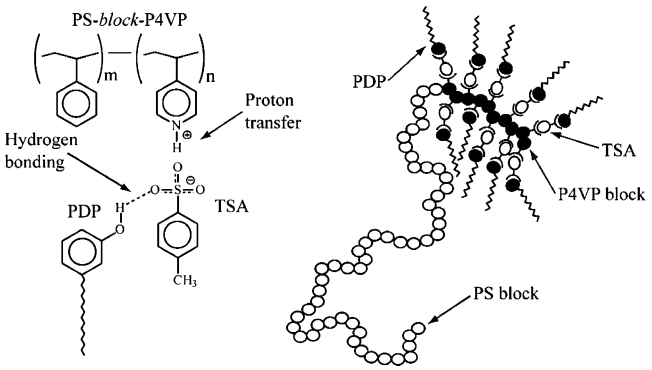

Figure 1. Schematics of the proposed interactions in the present work: protonation between toluenesulfonic acid (TSA) and the pyridines of polystyrene-*block*-poly(4-vinylpyridine) (PS-*block*-P4VP) as well as hydrogen bonding between pentadecylphenol (PDP) and sulfonates of the protonating TSA. Note also that uncomplexed pyridines of (PS-*block*-P4VP) are capable to form hydrogen bonds between PDP.[39] The shown scheme corresponds to the nominally complete complexation PS-*block*-P4VP(TSA)$_{0.9}$(PDP)$_{1.0}$.

structural hierarchy is reported, where the internal structure within the microphases is not perpendicular; in actual fact it is parallel to them. As the sizes of the microphases allow only few layers to be packed within them, the internal structure shows only relatively broad SAXS peaks. The anisotropy in conductivity is astonishingly small, only 1 order of magnitude, which may indicate that despite the overall alignment, the conducting nanochannels are not continuous.

2. Experimental Section

Materials and Sample Preparation. Polystyrene-*block*-poly(4-vinylpyridine) (PS-*block*-P4VP) was provided by Polymer Source Inc. and has the molecular weight of 41 400 and 1900 g/mol for the PS and P4VP blocks, and the polydispersity is 1.09. 3-*n*-Pentadecylphenol (PDP) obtained from Aldrich (purity 98 wt %) was further purified by recrystallizing twice using petrol ether. *p*-Toluenesulfonic acid monohydrate (TSA) (purity > 98.5 wt %) was purchased from Aldrich. Dilute (1 wt %) solutions from PS-*block*-P4VP, PDP, and TSA were first made using chloroform (Riedel-de Häen, purity 99 wt %). The solutions consisting of PS-*block*-P4VP and TSA were mixed to render PS-*block*-P4VP(TSA)$_{0.9}$. Thereafter, the PDP solution was added to lead the PS-*block*-P4VP(TSA)$_{0.9}$(PDP)$_{1.0}$. At the end, chloroform was evaporated at 60 °C for 2 h, and the sample was vacuum-dried at 25 °C for 48 h in 10^{-2} mbar.

FTIR Spectroscopy. The Fourier transform infrared measurements were performed at room temperature with Nicolet Magna 750 FTIR spectrometer averaging 64 scans with the resolution of 2 cm^{-1}. TSA, PDP, and the polymer complexes were ground and mixed with potassium bromide. KBr pellets were formed by pressing and before FTIR measurements the pellets were vacuum-dried at 25 °C for 28 h in 10^{-2} mbar vacuum.

Dynamic Rheological Orientation. A pellet of PS-*block*-P4VP(TSA)$_{0.9}$(PDP)$_{1.0}$ (diameter 10 mm, weight ca. 60 mg) was oriented by oscillatory shear flow using Bohlin CSM-50 stress controlled rheometer with a cone-and-plate geometry (the diameter of the cone is 11 mm and the angle is 4°). To obtain a homogeneous sample with a good contact to the rotor and to the stator of the rheometer, the pellet was first heated to 150 °C for approximately 10 min before shearing. Thereafter, oscillatory shear flow was imposed for ca. 9 h at 125 °C temperature,[37] which is sufficiently above the T_g of PS but still below the temperature where PDP becomes soluble in PS.[40] Frequency 0.05 Hz and strain amplitude 80% were selected due to the limitations of the rheometer.

Small-Angle X-ray Scattering. Pieces cut from the oriented pellets were studied using SAXS. Conventional sealed X-ray tube was used. Cu Kα radiation (wavelength $\lambda = 1.54$ Å) was monochromatized with a Ni filter and totally reflecting mirror within a Huber small-angle chamber 701. The incident beam was collimated to pointlike using slits. The distance between the sample and the 2-D detector (Bruker AXS) was 1200 mm, and the scattering vector range $q = 4\pi \sin\theta/\lambda$ is from 0.005 to 0.18 Å^{-1} where 2θ is the scattering angle. The pixel q values were calibrated using the silver behenate standard. Corrections for spatial distortion and flood field we made using a Fe-55 source and a SAXS 4.1.09-program (Bruker AXS, Karlsruhe, Germany). The measurements were made ex-situ with the incident beam in the tangential, radial, and normal directions using the cut pieces. The unoriented sample was also measured as a reference.

Modeling of the SAXS intensity in the plane normal to the hexagonally arranged microdomains was based on the following general formula[41]

$$I_{\perp}(q) = \langle F(\bar{q})\rangle^2(\langle S(\bar{q})\rangle - 1) + \langle F^2(\bar{q})\rangle \qquad (1)$$

where $F(\bar{q})$ is the structure factor for the individual microdomain cross section, $S(\bar{q})$ is the structure function of the hexagonal superlattice, $\bar{q}$ is the scattering vector in the plane, and the angle brackets denote azimuthal averaging. Calculation of F is based on known form factors,[42] and the azimuthal average was calculated numerically. The first term in (1) consists of sharp Bragg reflections, and the second term is scattering from the individual self-organized domains.

Transmission Electron Microscopy. For TEM, the unoriented sample and the samples cut from the oriented pellets were cast in epoxy and cured at 60 °C overnight. Sections in tangential and radial directions were cryomicrotomed at −120 °C, and the unoriented sample was microtomed at room temperature; sections were ca. 70 nm thick, and they were collected onto a 600 mesh size copper grid. Thereafter, sections were stained in I_2 for an hour to improve the contrast. Bright field TEM was performed using JEOL-1200EX transmission electron microscope operating at 60 kV accelerating voltage.

Conductivity Measurements. The conductivity of the oriented and vacuum-dried (25 °C, 24 h, 10^{-2} mbar) pellets were measured from the cut pieces (typical size 1 × 1.5 × 0.5 mm^3) in three directions with a Hewlett-Packard 4192LF impedance analyzer at frequencies 0.01−1000 kHz using a homemade conductivity cell and parallel plate geometry.[43] A Linkam TMS 91 heating stage was employed to produce the temperature cycle: room temperature (RT)−130 °C−60 °C−130 °C−60 °C−160 °C−60 °C−160 °C. The first heating from RT to 130 °C took place at a rate of 5 °C/min, and thereafter 1 °C/min was used in the subsequent cycling. After the first heating, the temperature was stopped for 5 min at 130 °C and subsequently at each temperature minima and maxima for a period of 3 min. Conductivity of the oriented PS-*block*-P4VP-(TSA)$_{0.9}$(PDP)$_{1.0}$ sample was measured in the tangential, radial, and normal direction. For comparison, also the conductivities of P4VP(TSA)$_{0.9}$(PDP)$_{1.0}$ and the unoriented PS-*block*-P4VP(TSA)$_{0.9}$(PDP)$_{1.0}$ were measured.

3. Results and Discussion

Complexation between TSA and P4VP was inferred from FTIR based on the characteristic carbon−nitrogen stretching. Figure 2 represents the FTIR spectra for the wavenumbers 1560−1700 cm^{-1} for TSA, PDP, PS-*block*-P4VP, PS-*block*-P4VP(TSA)$_{0.9}$, and PS-*block*-P4VP-(TSA)$_{0.9}$(PDP)$_{1.0}$ before and after the orientation. Pure P4VP has an absorption peak at wavenumbers 1596−1597 cm^{-1} due to the carbon−nitrogen stretching.[44−46] Upon complexation with a strong acid, the nitrogen becomes quaternized where the aromatic π cloud of pyridine becomes disturbed as the electron density shifts toward the nitrogen. Thus, the carbon−nitrogen bond is strengthened, and the remaining electron-deficient ring becomes even more electron-deficient. The rela-

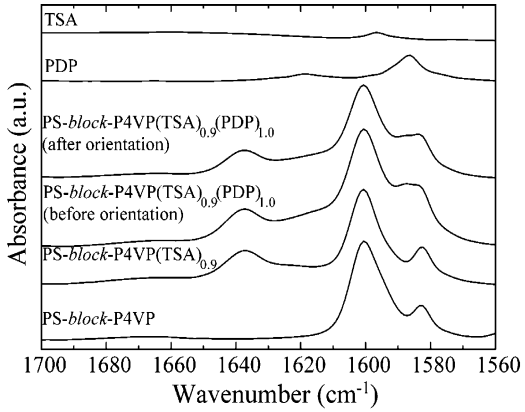

Figure 2. FTIR near 1600 cm^{-1}, showing the region of the pyridine ring stretching at 1597 cm^{-1} and the blue-shifted band of pyridinium at 1639 cm^{-1} due to proton transfer. Note the overlapping benzenoid absorption at 1600 cm^{-1}.

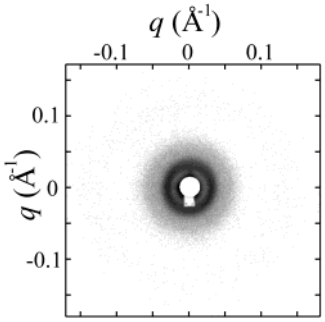

Figure 3. SAXS pattern of PS-*block*-P4VP(TSA)$_{0.9}$(PDP)$_{1.0}$ before the shear alignment, showing isotropic behavior where the SAXS patterns are similar in the three directions.

tively strong electron-withdrawing force due to the positive charge of nitrogen manifests as a large 40 cm^{-1} blue shift, and the peak is observed at 1637 cm^{-1}.[47] The blue shift is twice as large as observed for the coordination of the organometallic compounds of P4VP.[44,46] As the absorption peak near wavenumbers 1600 cm^{-1} is a composite peak, actually originating from the aromatic stretchings in both phenyls and uncomplexed pyridines, disappearance of the latter peak upon complexation cannot easily be quantitatively ascertained due to the strong overlap. As we wanted to minimize the amount of the uncomplexed acid and therefore only 0.9 mol of TSA was used vs for 1.0 mol of pyridine, the free pyridines remaining after the TSA complexation can form hydrogen bonds to PDP.[39] Figure 2 indicates also that orientation and shearing does not affect the protonation of the PS-*block*-P4VP(TSA)$_{0.9}$(PDP)$_{1.0}$. The complexation of PDP to the sulfonates of PS-*block*-P4VP(TSA)$_{0.9}$ cannot easily be studied using FTIR due to the complicated FTIR behavior of the sulfonate bands near 1200−1300 cm^{-1}. The hydrogen-bonding donor regime of the phenols above 3000 cm^{-1} indicated existence of hydrogen bondings, but the shifts could not be used to conclude bondings to the sulfonates, as PDP has a tendency to form also internal hydrogen bonds. Therefore, the hydrogen bonding between the sulfonates and PDP could be inferred only indirectly from SAXS.

The SAXS pattern for the unoriented sample at the q range 0.005−0.18 Å^{-1} is shown in Figure 3. A SAXS peak at $q \approx 0.03$ Å^{-1} is observed and the structure is isotropic, which is in a good agreement with a TEM image of the unoriented sample shown in Figure 4. After the shearing, the structure was studied ex-situ using

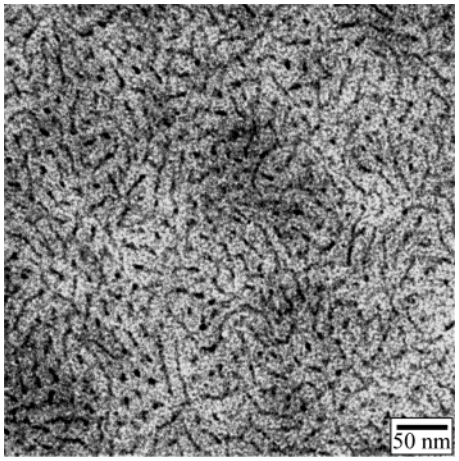

Figure 4. TEM image of unoriented PS-*block*-P4VP(TSA)$_{0.9}$-(PDP)$_{1.0}$ shows only local order.

SAXS in the tangential, radial, and normal directions relative to the flow (see Figure 5a−c). The data show sharp Bragg reflections in one plane only, which is orthogonal to the tangential direction (Figure 5a). The structure is hexagonal with a lattice constant of 235 Å, and the observed large number of higher order reflections suggests particularly good order. As the volume fraction of the polyelectrolytic P4VP(TSA)$_{0.9}$(PDP)$_{1.0}$ microphases is nominally roughly 0.20, their diameter could be estimated to be ca. 110 Å, if they were assumed to be cylindrical (which ultimately may be an oversimplification, to be discussed later). TEM confirms the overall alignment of the microphases along the shear flow as seen in Figure 6a,b. Note also that SAXS patterns in Figure 5 can be misleading, despite the high number of observed reflections; the TEM image in the tangential direction (Figure 6a) reveals that the material is still full of defects and domain boundaries. However, if the TEM image of Figure 6a is Fourier transformed (Image-Pro Plus version 4.1), one observes the characteristic six-pattern of hexagonal assembly (see the inset of Figure 6a), even showing second-order reflections. A closer look of TEM (Figure 6a) shows that shearing leads to approximately common alignment of the hexagonal domains even if domain boundaries remain, thus explaining the high number of SAXS reflections (Figure 5a). The smaller structure was not resolved using TEM, although previously in some other systems with higher molecular weight polymers we have been able to distinguish it.[17,18,40]

Figure 5b,c reveals another smaller structure, i.e., the existence of a structural hierarchy in the oriented material: A broad scattering peak is observed at ca. $q^* = 0.15$ Å^{-1}, corresponding to the long period $L_p = 2\pi/q^* = 41$ Å (see also Figure 7). A reflection at this q value has been observed previously (albeit much narrower) in homopolymeric P4VP(TSA)$_{1.0}$(PDP)$_{1.0}$[48] and in block copolymeric PS-*block*-P4VP(TSA)$_{1.0}$(PDP)$_{1.0}$[37] where higher order reflections indicated self-organized lamellar structure with alternating polyelectrolytic P4VP-(TSA) layers and PDP alkyl layers.[37] In the previously reported PS-*block*-P4VP(TSA)$_{1.0}$(PDP)$_{1.0}$[37] the block lengths differed from the present case with, in particular, a longer P4VP-block which resulted in a lamellar-*within*-lamellar structure with mutually perpendicular structures. These observations suggest to assign in the present case the observed broad reflection at $q^* = 0.15$ Å^{-1} (Figure 7) to similar self-organization. However, two

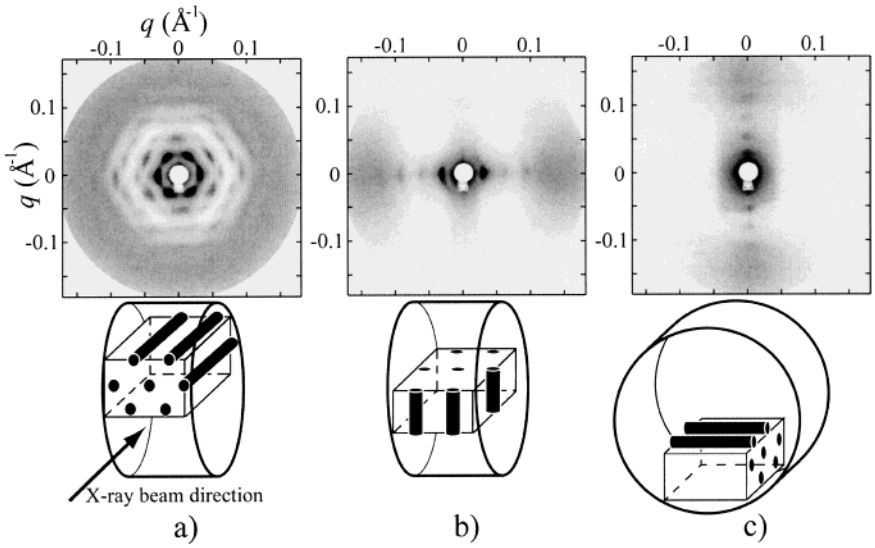

Figure 5. SAXS patterns for PS-*block*-P4VP(TSA)$_{0.9}$(PDP)$_{1.0}$. Ex-situ SAXS patterns after orientation (a) in the tangential direction, i.e., parallel to the flow; (b) in the radial direction; and (c) in the normal direction; the beam direction in (b) and (c) is held same as in (a).

specific features need to be additionally considered: the relative orientation of the two structures (Figure 5b,c) and the large width of the peak corresponding to the small structure. First, since the reflection is orthogonal to the tangential direction, it corresponds to structures *parallel* to the P4VP(TSA)$_{0.9}$(PDP)$_{1.0}$ microphases. Second, on the basis of the earlier studies,[37] it can be assumed that the structure is lamellar, although higher order peaks in this particular case are not observed. Therefore, more detailed models incorporating the structure factors of potential structures are needed. In fact, the orientation of the small structure and the large peak width are intimately connected. The lattice constant of the hexagonal structure is 235 Å, and as the volume fractions demand that the P4VP(TSA)$_{0.9}$(PDP)$_{1.0}$ microphases have cross-sectional dimensions of the order of half of that, it is sterically not possible to insert structures incorporating more than a few self-organized repeat units with periodicity of 41 Å in parallel to them. This would qualitatively explain the broad scattering peak.

Following these observations, possible alternatives of the hierarchical structures were considered. A successful model has to explain two observations: (i) the observed relative reflection intensities due to the hexagonal superstructure and (ii) the shape of the broad reflection due to the smaller structure.

Figure 7 shows the experimental azimuthally averaged and q-weighed diffraction intensity $I_{\perp}(q)$ in the plane normal to the hexagonal structure, as derived from the intensity pattern of Figure 5a. Potential layered structures were considered (see Figure 7 for the simplified schemes), which were denoted as the parallel two-layer model, parallel three-layer model, radial layer model, and cylindrical shell model. The experimental structure amplitudes $|F_{hk}|$ were determined by evaluating the areas under the Bragg reflections (h,k). These and the tail of intensity curve $I_{\perp}(q)$ were fitted to those calculated from the models based on eq 1. The layer thicknesses, cross-sectional dimensions of the microdomains, and the electron density differences between the different domains were adjustable parameters when searching a satisfactory fit to the experimental $I_{\perp}(q)$. Qualitative inspection of the shapes of the scattering patterns (Figure 7) suggests that only the two-layer model and the radial layer model need to be considered in more detail. The parallel layer models with three or four (not shown in Figure 7) layers suggest a much too narrow scattering peak.

Figure 7 shows that the parallel two-layer model with dimensions 84 Å × 126 Å reproduces the features of the scattering peak at $q = 0.1-0.2$ Å^{-1} well. The radial layer model reproduces the overall shape of the peak at 0.1−0.2 Å^{-1} satisfactorily, but the fit becomes poor for $q <$ 0.1 Å^{-1}. Note, however, that an artifact cannot be excluded when eq 1 is used where the total scattering intensity has been separated into contribution from the Bragg peaks and scattering from individual domains, which relies on the assumption of random orientation of the latter.

Figure 8 presents the relative amplitudes of the higher order diffraction peaks. For that purpose, the structure amplitudes $|F_{hk}|$ have been plotted as a function of q. The experimental values (black labels) are compared with values obtained based on the parallel layer (solid line) and the radial layer (dashed line) models. The three first diffraction peaks agree extremely well with both models. However, the parallel layer model fits better also in this case, in particular at the higher q values. Figures 7 and 8 encourage to consider the parallel two-layer model as a potential candidate for the aligned P4VP(TSA)$_{0.9}$(PDP)$_{1.0}$ microphases.

Figure 9 shows the conductivity values at 10 kHz as a function of temperature during the heating and cooling ramps. In general, the conductivity is very low. Because the instrument has a resolution of 10^{-9} S, the lowest conductivity values observed below 125 °C were not considered to be reliable, and only the values above 125 °C were taken into account to study the conductivity anisotropy in bulk matter. Figure 9 indicates that PS-*block*-P4VP(TSA)$_{0.9}$(PDP)$_{1.0}$ shows thermally activated conductivity in all directions. It may reflect a need of charge carrier hopping across boundaries in all directions and noncontinuous conducting channels despite alignment (see Figure 6b). The conductivity is anisotropic with the highest conductance along the cylinders.

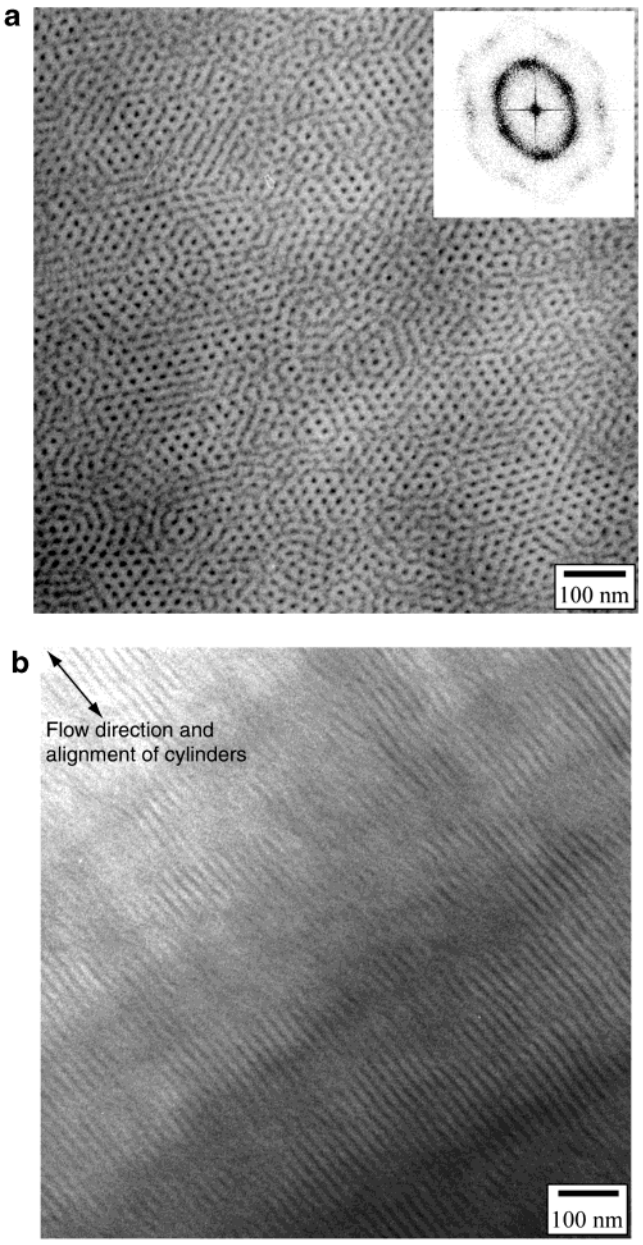

Figure 6. (a) TEM image of shear aligned PS-*block*-P4VP-(TSA)$_{0.9}$(PDP)$_{1.0}$ in the tangential direction. After the shearing a polydomain structure remains. Note however that the mutual orientations of the hexagonally assembled domains are correlated due to the shearing, thus leading to well-developed scattering patterns. The inset shows Fourier transformed TEM image where some distortion in the hexagonal pattern originates probably from the cutting compression due to the microtoming. (b) TEM image in the radial direction of the oriented PS-*block*-P4VP(TSA)$_{0.9}$(PDP)$_{1.0}$, clearly demonstrating the high overall orientation. The hexagonally packed microphases are aligned parallel to the flow direction.

Despite the good order, the anisotropy is astonishingly small, being only 1 order of magnitude. Note that a larger anisotropy is obtained in thin films (thicknesses ca. 50 nm) using hexagonally ordered PS-*block*-P4VP where the latter block has been alkylsulfonated.[49] We suggest that in our case the small anisotropy may result from still remaining defects and domain boundaries, which obstruct the continuous current flow and allows current to leak also perpendicular directions to aligned cylinders.

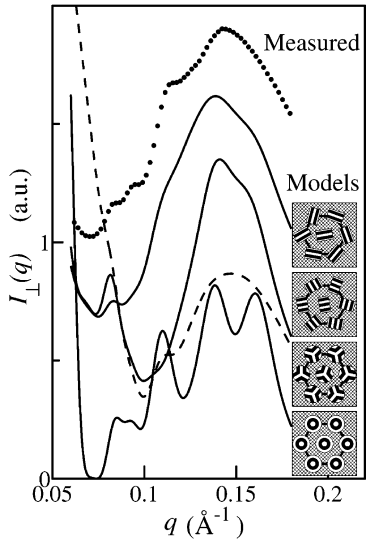

Figure 7. Measured azimuthally averaged and q-weighed SAXS intensity $I_\perp(q)$ obtained from the tangential measurement of PS-*block*-P4VP(TSA)$_{0.9}$(PDP)$_{1.0}$ shown in Figure 5a. The q value range relevant for the small structure has been selected near $q \approx 0.15$ Å^{-1}. Various models have been considered on the basis of the dimensions that give best fit to the observed data, in the order starting from the top: the parallel two-layer model where the size of the rectangular domains is 84 Å × 126 Å and the long period 42 Å which gave the best fit; the parallel three-layer model where the size of the rectangular domains is 81 Å × 123 Å with fitted 41 Å long period; the radial layer model where the cylinder radius is 51 Å, and the fitted long period is 39 Å; the concentric shell model where the cylinder radius is 134 Å. In the schemes: P4VP-(TSA)$_{0.9}$ layers are dark, PDP layers are white, and PS medium is gridded. The curves have been shifted for clarity.

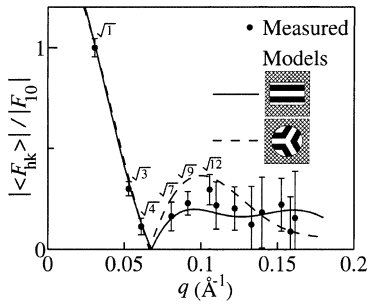

Figure 8. Measured relative structure amplitudes (dots) for the reflections (h,k) as determined from the tangential measurement of PS-*block*-P4VP(TSA)$_{0.9}$(PDP)$_{1.0}$ (see Figure 5a). Each dot represents the average of 6 or 12 equiv reflections for which the value $\sqrt{h^2+hk+k^2}$ is the same. The assignment of the lowest order peaks has been indicated for clarity. The error bars represent the 3σ limit. Starting from the top the two best fitting models are as follows: the parallel two-layer model where the size of the rectangular domains is 84 Å × 126 Å and the fitted long period is 42 Å; the radial layer model where the cylinder radius is 51 Å and the fitted long period is 39 Å. In the schemes: P4VP(TSA)$_{0.9}$ layers are dark, PDP layers white, and PS medium gridded.

4. Conclusion

We have achieved macroscopically highly aligned hexagonal morphology consisting of polyelectrolytic microphases within glassy PS matrix. The models fit to SAXS data suggest another level of layered parallel self-organization within the microphases. The macroscopic alignment is due to shear flow orientation performed at 125 °C with 0.05 Hz frequency and 80% strain amplitude. We observed slightly anisotropic electrical conductivity. The high overall order and the suggested

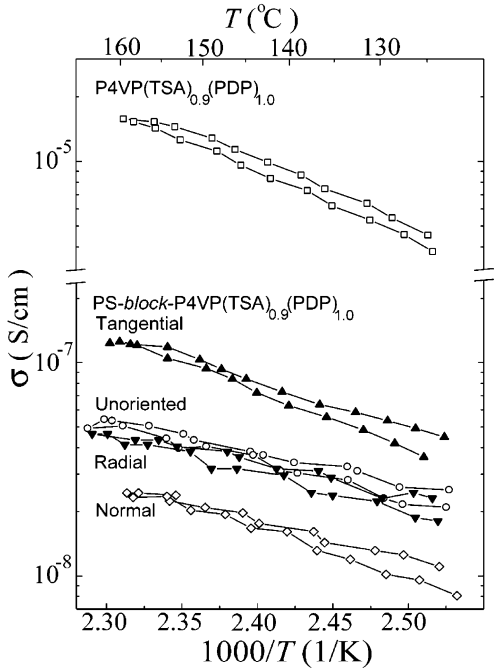

Figure 9. Ac conductivity of oriented PS-*block*-P4VP(TSA)$_{0.9}$-(PDP)$_{1.0}$ measured in the tangential, radial, and normal directions as a function of temperature. For comparison, also the conductivity of unoriented PS-*block*-P4VP(TSA)$_{0.9}$(PDP)$_{1.0}$ and P4VP(TSA)$_{0.9}$(PDP)$_{1.0}$ is shown.

novel morphology consisting of parallel nanochannels inside the self-organized microphases encourage to further developing of materials for functional purposes.

Acknowledgment. We thank Olli Lehtonen for discussions and calculations on interpretation of FTIR data. The financial support from the Academy of Finland and National Technology Agency (Finland) are gratefully acknowledged. This work was carried out in the Centre of Excellence of Finnish Academy ("Bio- and Nanopolymers Research Group", 77317). The Department of Electron Microscopy at the Institute of Biotechnology of Helsinki University is acknowledged for the use of their facilities.

References and Notes

(1) Whitesides, G. M.; Mathias, J. P.; Seto, C. T. *Science* **1991**, *254*, 1312.
(2) Muthukumar, M.; Ober, C. K.; Thomas, E. L. *Science* **1997**, *277*, 1225.
(3) Hamley, I. W. *The Physics of Block Copolymers*; Oxford University Press: Oxford, 1998.
(4) Bates, F. S.; Fredrickson, G. H. *Annu. Rev. Phys. Chem.* **1990**, *41*, 525.
(5) Ikkala, O.; ten Brinke, G. *Science* **2002**, *295*, 2407.
(6) Auschra, C.; Stadler, R. *Macromolecules* **1993**, *26*, 2171.
(7) Goldacker, T.; Abetz, V.; Stadler, R.; Erukhimovich, I.; Leibler, L. *Nature (London)* **1999**, *398*, 137.
(8) Bates, F. S.; Fredrickson, G. H. *Phys. Today* **1999**, *52*, 32.
(9) Abetz, V.; Goldacker, T. *Macromol. Rapid Commun.* **2000**, *21*, 16.
(10) Abetz, V. *Assemblies in Complex Block Copolymer Systems*; Marcel Dekker: New York, 2000.
(11) Adams, J.; Gronski, W. *Macromol. Chem., Rapid Commun.* **1989**, *10*, 553.
(12) Fischer, H.; Poser, S. *Acta Polym.* **1996**, *47*, 413.
(13) Stupp, S. I.; LeBonheur, V.; Walker, K.; Li, L. S.; Huggins, K. E.; Keser, M.; Amstutz, A. *Science* **1997**, *276*, 384.
(14) Jenekhe, S. A.; Chen, X. L. *Science* **1998**, *279*, 1903.
(15) Jenekhe, S. A.; Chen, X. L. *Science* **1999**, *283*, 372.
(16) Lee, M.; Cho, B.-K.; Zin, W.-C. *Chem. Rev.* **2001**, *101*, 3869.
(17) Ruokolainen, J.; Mäkinen, R.; Torkkeli, M.; Mäkelä, T.; Serimaa, R.; ten Brinke, G.; Ikkala, O. *Science* **1998**, *280*, 557.
(18) Ruokolainen, J.; ten Brinke, G.; Ikkala, O. T. *Adv. Mater.* **1999**, *11*, 777.
(19) Thünemann, A. F.; General, S. *Macromolecules* **2001**, *34*, 6978.
(20) Kosonen, H.; Valkama, S.; Hartikainen, J.; Eerikäinen, H.; Torkkeli, M.; Jokela, K.; Serimaa, R.; Sundholm, F.; ten Brinke, G.; Ikkala, O. *Macromolecules* **2002**, *35*, 10149.
(21) Kosonen, H.; Valkama, S.; Ruokolainen, J.; Torkkeli, M.; Serimaa, R.; ten Brinke, G.; Ikkala, O. *Eur. Phys. J.* **2003**, *10*, 69.
(22) Valkama, S.; Ruotsalainen, T.; Kosonen, H.; Ruokolainen, J.; Torkkeli, M.; Serimaa, R.; ten Brinke, G.; Ikkala, O. *Macromolecules* **2003**, *36*, 3986.
(23) Osuji, C.; Chao, C.-Y.; Bita, I.; Ober, C. K.; Thomas, E. L. *Adv. Funct. Mater.* **2002**, *12*, 753.
(24) Mäki-Ontto, R.; de Moel, K.; de Odorico, W.; Ruokolainen, J.; Stamm, M.; ten Brinke, G.; Ikkala, O. *Adv. Mater.* **2001**, *13*, 117.
(25) Alberda van Ekenstein, G.; Polushkin, E.; Nijland, H.; Ikkala, O.; ten Brinke, G. *Macromolecules* **2003**, *36*, 3684.
(26) Knoll, A.; Horvat, A.; Lyakhova, K. S.; Krausch, G.; Sevink, G. J. A.; Zvelindovsky, A. V.; Magerle, R. *Phys. Rev. Lett.* **2002**, *89*, 035501.
(27) Thurn-Albrecht, T.; Schotter, J.; Kästle, G. A.; Emley, N.; Shibauchi, T.; Krusin-Elbaum, L.; Guarini, K.; Black, C. T.; Tuominen, M. T.; Russell, T. P. *Science* **2000**, *290*, 2126.
(28) Thurn-Albrecht, T.; Steiner, R.; DeRouchey, J.; Stafford, C. M.; Huang, E.; Bal, M.; Tuominen, M.; Hawker, C. J.; Russell, T. P. *Adv. Mater.* **2000**, *12*, 787.
(29) Schäffer, E.; Thurn-Albrecht, T.; Russell, T. P.; Steiner, U. *Nature (London)* **2000**, *403*, 874.
(30) Böker, A.; Knoll, A.; Elbs, H.; Abetz, V.; Mueller, A. H. E.; Krausch, G. *Macromolecules* **2002**, *35*, 1319.
(31) Böker, A.; Elbs, H.; Hänsel, H.; Knoll, A.; Ludwigs, S.; Zettl, H.; Urban, V.; Abetz, V.; Mueller, A. H. E.; Krausch, G. *Phys. Rev. Lett.* **2002**, *89*, 135502.
(32) Hamley, I. W. *J. Phys.: Condens. Matter.* **2001**, *13*, 643.
(33) Chen, Z.-R.; Kornfield, J. A.; Smith, S. D.; Grothaus, J. T.; Satkowski, M. M. *Science* **1997**, *277*, 1248.
(34) Sänger, J.; Gronski, W.; Leist, H.; Wiesner, U. *Macromolecules* **1997**, *30*, 7621.
(35) Zhang, Y.; Wiesner, U. *J. Chem. Phys.* **1997**, *106*, 2961.
(36) Mäkinen, R.; Ruokolainen, J.; Ikkala, O.; de Moel, K.; ten Brinke, G.; De Odorico, W.; Stamm, M. *Macromolecules* **2000**, *33*, 3441.
(37) Mäki-Ontto, R.; de Moel, K.; Polushkin, E.; Alberda van Ekenstein, G.; ten Brinke, G.; Ikkala, O. *Adv. Mater.* **2002**, *14*, 357.
(38) Jen, K.-Y.; Elsenbaumer, R. L. Thermally stable forms of electrically conductive polyaniline. U.S. Patent 5,456,862, 1995.
(39) Ruokolainen, J.; ten Brinke, G.; Ikkala, O.; Torkkeli, M.; Serimaa, R. *Macromolecules* **1996**, *29*, 3409.
(40) Ruokolainen, J.; Saariaho, M.; Ikkala, O.; ten Brinke, G.; Thomas, E. L.; Torkkeli, M.; Serimaa, R. *Macromolecules* **1999**, *32*, 1152.
(41) Tadokoro, H. *Structure of Crystalline Polymers*; John Wiley & Sons: New York, 1979.
(42) Pedersen, J. S. *Adv. Colloid Interface Sci.* **1997**, *70*, 171.
(43) Ruotsalainen, T.; et al. To be published.
(44) Peiffer, P. D.; Duvdevani, I.; Agarwal, P. K. *J. Polym. Sci., Polym. Lett. Ed.* **1986**, *24*, 581.
(45) Pires, A. T. N.; Cheng, C.; Belfiore, L. A. *Polym. Mater. Sci. Eng.* **1989**, *61*, 466.
(46) Belfiore, L. A.; Pires, A. T. N.; Wang, Y.; Graham, H.; Ueda, E. *Macromolecules* **1992**, *25*, 1411.
(47) Ikkala, O.; Ruokolainen, J.; ten Brinke, G.; Torkkeli, M.; Serimaa, R. *Macromolecules* **1995**, *28*, 7088.
(48) Ikkala, O.; Ruokolainen, J.; Torkkeli, M.; Tanner, J.; Serimaa, R.; ten Brinke, G. *Colloids Surf. A* **1999**, *147*, 241.
(49) Cho, G.; Park, K.-P.; Jang, J.; Jung, S.; Moon, J.; Kim, T. *Electrochem. Commun.* **2002**, *4*, 336.

MA0345955